Developmental Cell, Vol. 2, 55–67, January, 2002, Copyright ©2002 by Cell Press

A Distinct Pathway Remodels Mitochondrial Cristae and Mobilizes Cytochrome *c* during Apoptosis

Luca Scorrano,[1] Mona Ashiya,[1] Karolyn Buttle,[2] Solly Weiler,[1] Scott A. Oakes,[1] Carmen A. Mannella,[2] and Stanley J. Korsmeyer[1,3]

[1] Howard Hughes Medical Institute
Department of Pathology and Medicine
Harvard Medical School
Dana Farber Cancer Institute
Boston, Massachusetts 02115

[2] Resource for the Visualization of Biological Complexity
Wadsworth Center
Empire State Plaza
Albany, New York 12201

Summary

The mechanism during apoptosis by which cytochrome *c* is rapidly and completely released in the absence of mitochondrial swelling is uncertain. Here, we show that two distinct pathways are involved. One mediates release of cytochrome *c* across the outer mitochondrial membrane, and another, characterized in this study, is responsible for the redistribution of cytochrome *c* stored in intramitochondrial cristae. We have found that the "BH3-only" molecule tBID induces a striking remodeling of mitochondrial structure with mobilization of the cytochrome *c* stores (~85%) in cristae. This reorganization does not require tBID's BH3 domain and is independent of BAK, but is inhibited by CsA. During this process, individual cristae become fused and the junctions between the cristae and the intermembrane space are opened.

Introduction

The mitochondrion is a prominent participant in apoptosis following a variety of death stimuli (Green and Reed, 1998; Kroemer et al., 1998). The "multidomain" proapoptotic BCL-2 family members BAX and BAK prove necessary for the onset of mitochondrial dysfunction and cell death following remarkably diverse signals (Wei et al., 2001). Thus, the mitochondrion may prove an obligate organelle for apoptosis downstream of perhaps all intrinsic pathway signals. Release of cytochrome *c* from the intermembrane space (IMS) is a prominent facet of such intrinsic pathway deaths. Cytochrome *c* triggers a postmitochondrial pathway, forming an "apoptosome" of Apaf-1, cytochrome *c*, and caspase-9, which subsequently cleaves the effector caspases -3 and -7 (Li et al., 1997).

The precise mechanism whereby cytochrome *c* is released across the outer mitochondrial membrane (OM) is less certain. Permeability transition (PT) that ultimately leads to mitochondrial swelling with secondary rupture of the OM and cytochrome *c* release has been noted in certain apoptotic and necrotic deaths (Lemasters et al., 1998). In its fully open conformation, the PT pore (PTP), a high-conductance inner membrane channel, is permeable to solutes up to 1500 Da (Bernardi, 1999). However, openings of the PTP can also be transient and not cause swelling (Huser et al., 1998; Petronilli et al., 1999). As originally noted at the single-channel level, the PTP flickers over msecs between open and closed states (Petronilli et al., 1989). Cyclosporin A (CsA) inhibits both activities of the PTP, presumably through its mitochondrial target cyclophilin D (Nicolli et al., 1996). Thus, models of cytochrome *c* release must also assess whether PT participates.

Defining the serial events responsible for cytochrome *c* release requires a distinct initiating event. The "BH3-only" subset of BCL-2 members provides such a signal, as they connect proximal death signals to the core apoptotic pathway at the mitochondria. The "BH3-only" molecules BID, BAD, BIM, and NOXA require the "multidomain" members BAX and BAK to release cytochrome *c* and induce cell death (Wei et al., 2001; Zong et al., 2001; Cheng et al., 2001). For example, after CD95 (Fas) or TNFR1 engagement, BID is cleaved by caspase-8 followed by N-myristoylation to induce its molecular activation (Luo et al., 1998; Zha et al., 2000). Recombinant tBID is an ideal initiating event, as it appears to function as a death ligand that induces the homooligomerization of BAK with subsequent release of cytochrome *c* from wt but not *Bak*-deficient mitochondria (Wei et al., 2000). tBID releases cytochrome *c* without detectable swelling of the mitochondria (Shimizu and Tsujimoto, 2000; Eskes et al., 1998), but increases the permeability of the OM (Kluck et al., 1999).

Any model must also account for the rapid kinetics and complete extent of cytochrome *c* release (Goldstein et al., 2000). High-voltage electron microscopic (HVEM) tomography of mitochondria has revealed that the IMS is very narrow, as the average distance between the outer (OM) and inner (IM) boundary membranes is only ~20 nm (Frey and Mannella, 2000), consistent with functional estimates that only 15%–20% of total cytochrome *c* is available in the IMS (Bernardi and Azzone, 1981). The pleomorphic, tubular cristae constitute highly sequestered compartments, where the majority of oxidative phosphorylation complexes (Perotti et al., 1983) and cytochrome *c* is separated from the IMS by narrow cristae junctions. A major challenge is to explain how this compartmentalized store of cytochrome *c* can be released in the absence of mitochondrial swelling. Therefore, we investigated whether a structural reorganization occurs during apoptosis to mobilize the cristae stores of cytochrome *c* for release across the OM.

Results

tBID Treatment, Unlike Selective Solubilization of the Outer Membrane, Results in Complete Release of Cytochrome *c*

We determined the kinetics and extent of tBID-induced release of cytochrome *c*. Recombinant tBID displayed

[3] Correspondence: stanley_korsmeyer@dfci.harvard.edu

a dose-dependent release of cytochrome *c* from mitochondria, reaching a plateau at higher tBID concentrations after 45 min (Figures 1A and 1C). At the concentration of 320 pmol tBID per 1.0 mg of mitochondrial protein, tBID integration into mitochondrial membranes maximized after 15 min, while at lower concentrations, it was complete only after 45 min (data not shown). Cytochrome *c* release increased in a time-dependent manner at the maximum tBID concentration (Figures 1B and 1D). Complete cytochrome *c* release was also observed with 0.32 pmol $\times$ mg protein^{-1} of myristoylated p7/p15 BID complex (due to its enhanced mitochondrial targeting; data not shown). These experiments show that tBID releases almost all the mitochondrial cytochrome *c* in a concentration- and time-dependent manner.

Mitochondria were incubated with increasing amounts of digitonin to assess how much cytochrome *c* was released from IMS by the selective solubilization of the OM (Hoppel and Cooper, 1968). To monitor interaction of digitonin with the IM, we assessed uncoupled respiration in the presence of excess exogenous cytochrome *c*. Approximately 16% of the total cytochrome *c* could be released by digitonin without substantial respiratory inhibition (no interference of digitonin with the IM; Table 1), a percentage in agreement with the pool of cytochrome *c* estimated to reside in the IMS (Bernardi and Azzone, 1981). Therefore, tBID must deploy additional events to enable the release of nearly all cytochrome *c* from the mitochondrion.

We next evaluated whether tBID causes any swelling or depolarization that might reflect an opening of the PTP. tBID did not induce appreciable mitochondrial swelling over 60 min, while a slight depolarization was recorded (Figure 1E), consistent with prior observations (Wei et al., 2000; Shimizu and Tsujimoto, 2000; Kluck et al., 1999; von Ahsen et al., 2000). However, openings of the PTP can also be transient (Petronilli et al., 1999), with no alterations in membrane potential or light scattering (Bernardi et al., 1999) and can be assessed in mitochondrial populations by following the release of a matrix-entrapped fluorophore, calcein (Huser et al., 1998). tBID causes a time-dependent increase in the release of matrix calcein and CsA completely inhibits this effect of tBID (Figure 1F). These experiments indicate that tBID induces a CsA-sensitive calcein release; however, this is not accompanied by any mitochondrial large amplitude swelling that could rupture the OM and account for the complete release of cytochrome *c*.

CsA Does Not Alter BAK Oligomerization, but Does Diminish Release of Cytochrome *c* and Adenylate Kinase

tBID induces a time-dependent appearance of higher order BAK oligomers that was not affected by CsA (Figure 2A). Consequently, we then assessed whether CsA would alter the kinetics or extent of tBID-induced cytochrome *c* release. As a control, a blocking anti-BAK antibody did completely prevent cytochrome *c* release (Figure 2B). However, CsA only partially interfered with tBID-induced release of cytochrome *c* (Figure 2B). We sought to determine whether a similar pattern resulted for additional proteins that are released from the mitochondria during apoptosis, such as the $\sim$26 kDa adenylate kinase (AK; Single et al., 1998). tBID induced the release of AK, and anti-BAK antibody also completely inhibited that release. CsA substantially decreased but did not completely eliminate release of AK, similar to the release of cytochrome *c* (Figure 2C). Neither anti-BCL-X_L antibody nor the broad specificity caspase inhibitor zVAD-fmk had any effect on tBID-induced release of cytochrome *c* or AK (data not shown). These experiments reveal that BAK oligomerization, which is essential for tBID-induced cytochrome *c* release, still occurs in the presence of CsA. Consistent with this observation, some cytochrome *c* and AK is still released, however substantial stores are retained, indicating CsA blocks a significant component of the tBID pathway.

CsA blocked tBID-induced transient opening of the PTP, but not BAK oligomerization or the initial release of cytochrome *c*, suggesting that these processes are distinct. Therefore, we turned to *Bak*-deficient mitochondria to determine their response. tBID did not induce significant cytochrome *c* release across the outer membrane of *Bak*$^{-/-}$ as contrasted with wt mitochondria (data not shown; Wei et al., 2000). In contrast, tBID induced comparable CsA-inhibitable calcein release in *Bak*$^{-/-}$ as well as *wt* mitochondria (Figure 2D). These data indicate that the tBID-induced calcein release is BAK independent, but is fully sensitive to CsA. Moreover, sustained flickering of the PTP is not secondary to the loss of cytochrome *c*, since *Bak*$^{-/-}$ mitochondria do not release cytochrome *c*.

tBID Results in a BAK-Independent, CsA-Sensitive Redistribution of Cytochrome *c* into the Intermembrane Space

The amount of cytochrome *c* released at 15 min in the presence of tBID plus CsA was $\sim$17% more than buffer alone (Figure 2B), similar to the estimate ($\sim$16%) of cytochrome *c* that is resident in the IMS. The precise mechanism whereby the stores of cytochrome *c* within the cristae ($\sim$85%) are mobilized for release during apoptosis remained uncertain. Therefore, we examined whether tBID induced redistribution of cytochrome *c* stores from the cristae to the IMS, where it would be available for release across the OM in a BAK-dependent fashion. We developed assays to assess the amount of cytochrome *c* freely available in the IMS (Figures 3A and 3B). Ascorbate is capable of reducing only free cytochrome *c*, whereas the uncharged reductant TMPD is membrane permeable and diffuses widely to reach all cytochrome *c* (Nicholls et al., 1980). Consequently, the ratio of ascorbate-driven respiration over the total TMPD-driven respiration (ascorbate/TMPD) would be expected to increase if cytochrome *c* was mobilized. In support, unfolding of the cristae caused by Ca^{2+}-mediated swelling increases the ascorbate-driven respiration (Figure 3C). tBID caused a substantial increase in ascorbate-driven respiration at 15 min that was blocked by pretreatment with CsA (Figures 3C and 3D). This increase occurred independently of BAK (Figure 3D). These experiments indicate tBID treatment dissociates cytochrome *c* from its ascorbate-inaccessible sites.

We then quantitated the accessibility of cytochrome *c* to the OM by measuring the effects of tBID on cytochrome b_5-mediated NADH oxidation (Figures 3A and

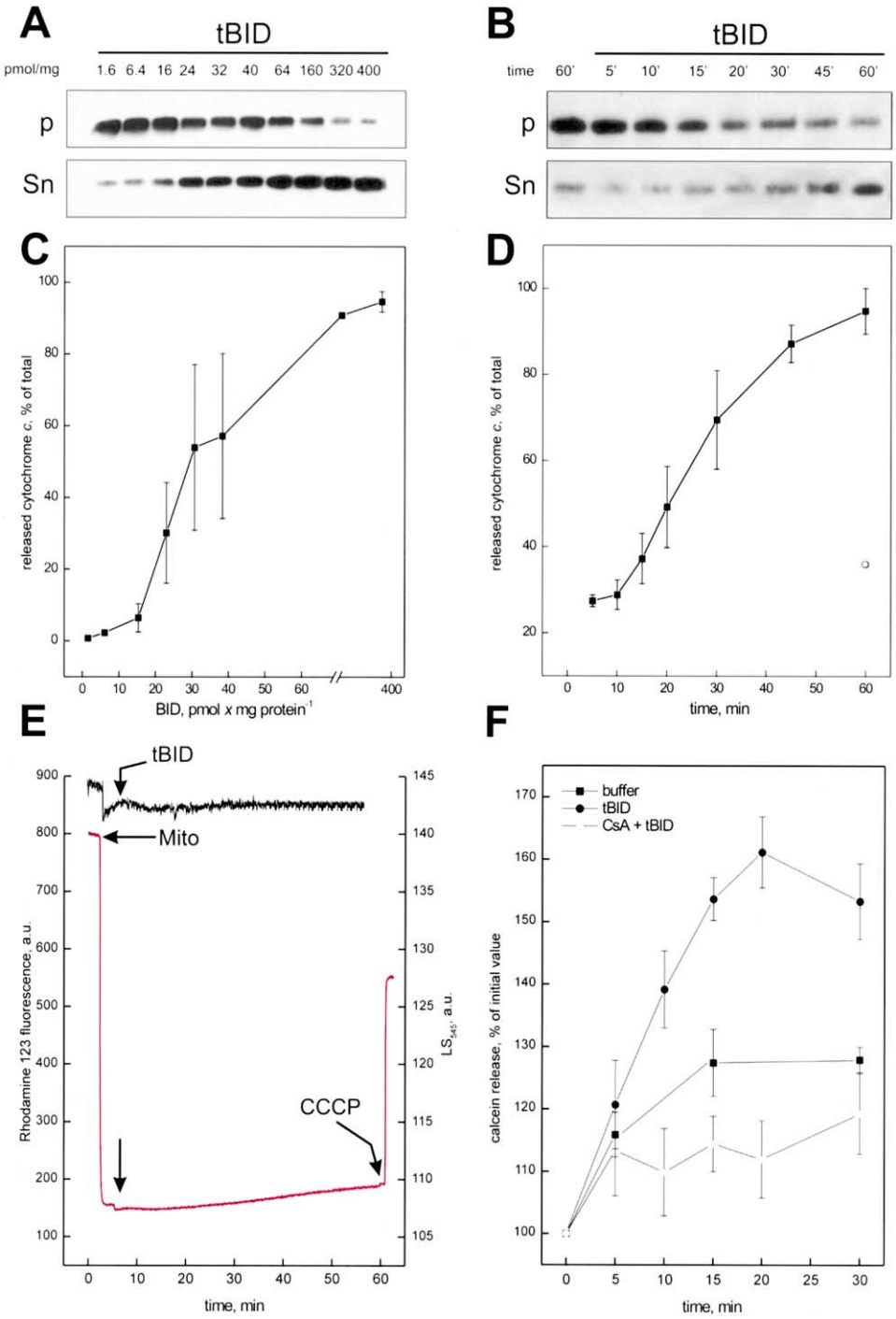

Figure 1. tBID-Induced Cytochrome *c* Release and Effects on Light Scattering, Mitochondrial Membrane Potential, and Calcein Release

(A and B) Representative immunoblot of cytochrome *c* in pellets (p) and supernatants (sn) of mitochondria treated for 45 min with the indicated concentration of tBID (A) or with 320 pmol tBID × mg protein^{-1} for the indicated time (B).

(C) Concentration dependence of tBID-induced cytochrome *c* release.

(D) Time course of cytochrome *c* release by tBID. In (C) and (D), data derived from densitometry of immunoblots represent mean ± SD of three different experiments.

(E) Effects of tBID on light scattering and membrane potential. 0.5 mg/ml mitochondria was incubated in experimental buffer supplemented with 0.3 μM rhodamine 123 (red trace only). Where indicated (arrows), tBID and 400 pmol CCCP × mg protein^{-1} were added. The drop in rho 123 fluorescence is caused by the addition of mitochondria.

(F) Release of matrix-entrapped calcein by tBID. 0.5 mg/ml of calcein-loaded mitochondria was incubated for the indicated time with tBID (closed and open circles). Open circles, mitochondria were pretreated for 2 min with 800 pmol CsA × mg protein^{-1}; squares, no tBID. Data represent mean ± SD of five different experiments.

Table 1. Effects of Digitonin on Cytochrome *c* Release and Respiration

Digitonin (pmol × mg protein^{-1})	0	48	80	145
Cytochrome *c* release (% of total)	5.2	10.7	16.4	26.6
Uncoupled J_{O_2} (nAt × min^{-1} × mg protein^{-1})	66.9	60	60	46.7

0.5 mg/ml mitochondria was incubated in EB with the indicated concentration of digitonin. After 5 min, mitochondria were centrifuged and cytochrome *c* content in the resulting pellet and supernatant was determined as described. Uncoupled J_{O_2}, uncoupled respiratory rate was recorded in parallel experiments. After 5 min of incubation with the indicated concentration of digitonin, mitochondria were treated with 400 pmol CCCP × mg protein^{-1} in the presence of 10 nmol cytochrome *c* × mg protein^{-1}.

3B). Cytochrome b_5 is an OM protein that transfers electrons from an NADH dehydrogenase, accessible to exogenous (i.e., extramitochondrial) NADH, to cytochrome *c* (Lehninger, 1951; Bernardi and Azzone, 1981). The availability of cytochrome *c* is rate limiting for this reaction. The NADH oxidation rate increases when more cytochrome *c* is available to cytochrome b_5, reflecting more cytochrome *c* present in the IMS (Bernardi and Azzone, 1981). As the model predicts (Figures 3A and 3B), treatment of mitochondria with Ca^{2+} increased the rate of NADH oxidation, as a consequence of the cristae unfolding that accompanies mitochondrial swelling (Figures 3B and 3E). The NADH oxidation in this assay is completely dependent on cytochrome b_5, since assays were performed in the presence of the complex I inhibitor rotenone, and all increases proved completely inhibited by the cytochrome b_5 inhibitor mersalyl (Bernardi and Azzone, 1981; Figures 3A and 3E). tBID also increased the NADH oxidation rate, which proved fully inhibitable by CsA (Figure 3E). We next examined cytochrome b_5-dependent NADH oxidation in *Bak*$^{-/-}$ mitochondria. tBID induced a comparable, CsA-inhibitable, increase in cytochrome b_5-dependent NADH oxidation in BAK-deficient mitochondria (Figure 3F). This similar increase in *wt* and *Bak*$^{-/-}$ mitochondria eliminates the possibility that the released cytochrome *c* might accept electrons at the cytochrome b_5 site.

We also asked whether tBID would increase the amount of cytochrome *c* available for release as tested by detergent permeabilization of the OM of *Bak*$^{-/-}$ mitochondria. Treatment of *Bak*$^{-/-}$ mitochondria with a concentration of digitonin that does not interfere with IM function caused the release of 19.2 ± 4.8% of total cytochrome *c* (Figure 3G). Pretreatment of *Bak*$^{-/-}$ mitochondria with tBID increased the amount of cytochrome *c* released to levels comparable to that of wt mitochondria. This tBID-induced mobilization was also CsA inhibitable (Figure 3G). Thus, three assay systems indicate that tBID causes a BAK-independent mobilization of cytochrome *c* that increases its availability for release across the OM.

BH3 of tBID Is Required for Cytochrome *c* Release, but Not Cytochrome *c* Mobilization or Transient Permeability Transition

The conserved amphipathic α-helical BH3 domain is required for the full biologic activity of the "BH3-only" molecules. tBID requires an intact BH3 domain to bind BAK, induce the oligomerization of BAK, and release cytochrome *c* (Wei et al., 2000). We tested the BH3 mutant BID G94E, which targets mitochondria but fails to release cytochrome *c*, for its ability to induce transient opening of the PTP. BID G94E proved as effective as wt BID in inducing the release of calcein (Figure 2E). Moreover, examination of cytochrome b_5-dependent NADH oxidation indicates that mutant G94E increased cytochrome *c* accessibility to the OM nearly as well as wt BID (Figure 3H). This provides further evidence that the release of cytochrome *c* across the OM (BH3-dependent) is a separable pathway from the mobilization of cytochrome *c* (BH3-independent). Moreover, it indicates that a region of tBID beyond BH3, likely an intramembranous portion, is responsible for triggering the mobilization of cytochrome *c*.

tBID Induces the Remodeling of Mitochondrial Cristae, Accounting for the Mobilization of Cytochrome *c* in a BAK-Independent, CsA-Inhibitable Pathway

The physiological assays employed above identified an induced redistribution of cytochrome *c*, presumably from the cristae into the IMS. This BAK-independent, CsA-inhibitable redistribution of cytochrome *c* is distinct from the release of cytochrome *c* across the OM, as BAK-deficient mitochondria redistribute, but do not release, cytochrome *c*. To determine whether structural changes to mitochondria accompanied these physiologic measurements of cytochrome *c* mobilization, we collected transmission electron microscopic (TEM) images (Figure 4). Purified normal mitochondria in the presence of respiratory substrates display a partially condensed conformation we refer to as class I morphology, with numerous narrow pleomorphic cristae (appearing in TEM as small electron-transparent areas) in a contiguous electron-dense matrix space (Figures 4A, 4D, and 5A). tBID-treated mitochondria display a series of morphological changes. The majority of the mitochondrial population appears to be in a remodeled state we denote as class II, characterized by a serpentine electron-transparent intracristal compartment interrupted by electron-dense matrix spaces (Figures 4B, 4E, and 5A). The electron-dense matrix often appears circular and, depending on the orientation of the thin section, can be organized to resemble an "intestinal" or "sausage-shaped" electron-dense region. Remodeled class II mitochondria differ from the condensed mitochondria described by Hackenbrock during stimulated (state 3; Hackenbrock, 1966) respiration, in that the cristae and matrix spaces are markedly reorganized. Moreover, addition of excess ADP to our isotonic respiratory buffer did not cause the appearance of class II mitochondria (data not shown). A few tBID-treated mitochondria have progressed to gross morphological derangement entitled class III, with asymmetric blebbing of herniated matrix resulting in a partial rupture of the OM and swelling on one side of the mitochondrion (Figure 5A). A class IV designation was assigned to a terminally swollen and ruptured mitochondrion with little or no distinguishable cristae structure (Figure 5A). The mean calculated area of 100 measured class II mitochondria was comparable to that of 100 class I mitochondria (2.14 versus 2.38 μm^2; ANOVA test; ns), arguing that as a population, they are not swollen. These same stages are also observed in

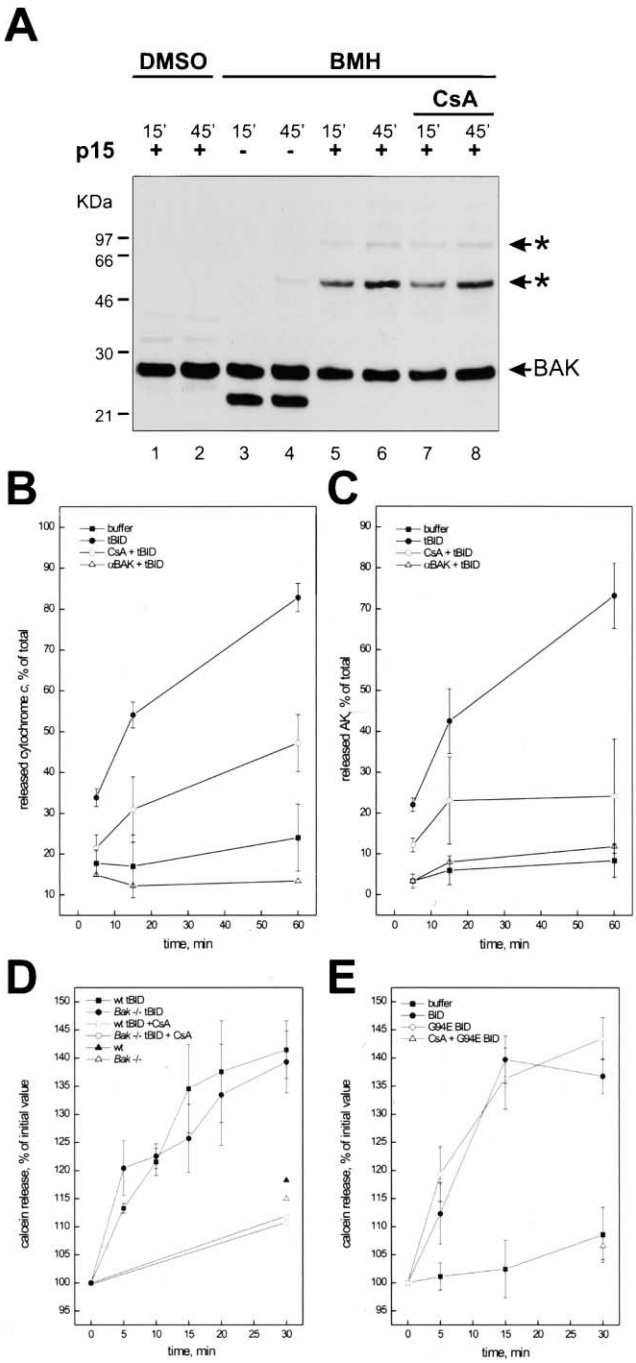

Figure 2. Regulation of tBID-Induced Release of Cytochrome *c* and Adenylate Kinase versus Release of Calcein

(A) tBID induces CsA-insensitive BAK oligomerization. 0.5 mg/ml mitochondria was incubated with tBID (lanes 1, 2, 5, and 6). In lanes 7 and 8, mitochondria were pretreated with 800 pmol CsA × mg protein^{-1} for 3 min. After the indicated time, DMSO (lanes 1 and 2) or 10 mM BMH (lanes 3–8) was added, and after another 30 min the crosslinking reaction was quenched (Wei et al., 2001). The mitochondria were subjected to SDS-PAGE and immunoblot with anti-BAK antibody. Asterisk, BAK multimers.

(B and C) Quantification of the effects of CsA and of blocking anti-BAK antibodies on tBID-induced cytochrome *c* and adenylate kinase (AK) release. In both panels, mitochondria were incubated for the indicated time in the absence (closed squares) or presence of tBID (closed circles). Open circles, mitochondria preincubated for 2 min with 800 pmol CsA × mg protein^{-1}; open triangles, mitochondria preincubated for 30 min with 0.1 μg × mg protein^{-1} anti-BAK Ab. Data represent mean ± SD of four different experiments.

(D) tBID-induced calcein release in *wt* and *Bak*$^{-/-}$ mitochondria. 0.5 mg/ml of calcein-loaded *wt* (squares) or *Bak*$^{-/-}$ (circles) mitochondria were incubated for the indicated time with tBID (closed symbols). Open symbols indicate no tBID.

(E) Effects of a G94E BID mutant on calcein release. The experiment was performed as in (A), except that wt (closed circles) or G94E (open circles) p7/p15 BID complex was used. Squares, no BID; triangles, mitochondria incubated with 800 pmol CsA × mg protein^{-1} for 3 min before the addition of BID.

tBID-treated *Bak*$^{-/-}$ mitochondria (Figure 4E). However, pretreatment with CsA inhibits the appearance of these abnormalities (Figures 4C and 4F).

Since both the redistribution of cytochrome *c* and its release across the OM are functions of time, we performed morphometric analysis on mitochondria over a time course following addition of tBID. tBID induced a shift in mitochondrial morphology from class I to class II within 2 min, and by 5 min, class II mitochondria predominate (Figures 5B and 5C). At later time points, class III and class IV mitochondria appear in vitro (Figure 5D). While this tBID-induced morphologic progression also occurs in the absence of BAK, it is inhibited by treatment with CsA (Figure 5). Overall, the time course of appearance of class II mitochondria temporally correlates with the redistribution of cytochrome *c*, and both proved sensitive to CsA.

To determine whether class II morphology could account for the increased availability of cristae stores of cytochrome *c* required a three-dimensional reconstruction of such mitochondria. We employed high-voltage electron microscopy (HVEM) and tomographic reconstruction performed on thick sections of mitochondria. Selected surface-rendered views of representative tomographic reconstructions belonging to class I–III mitochondria (Figures 6A–6C) are presented in Figures 6A′,

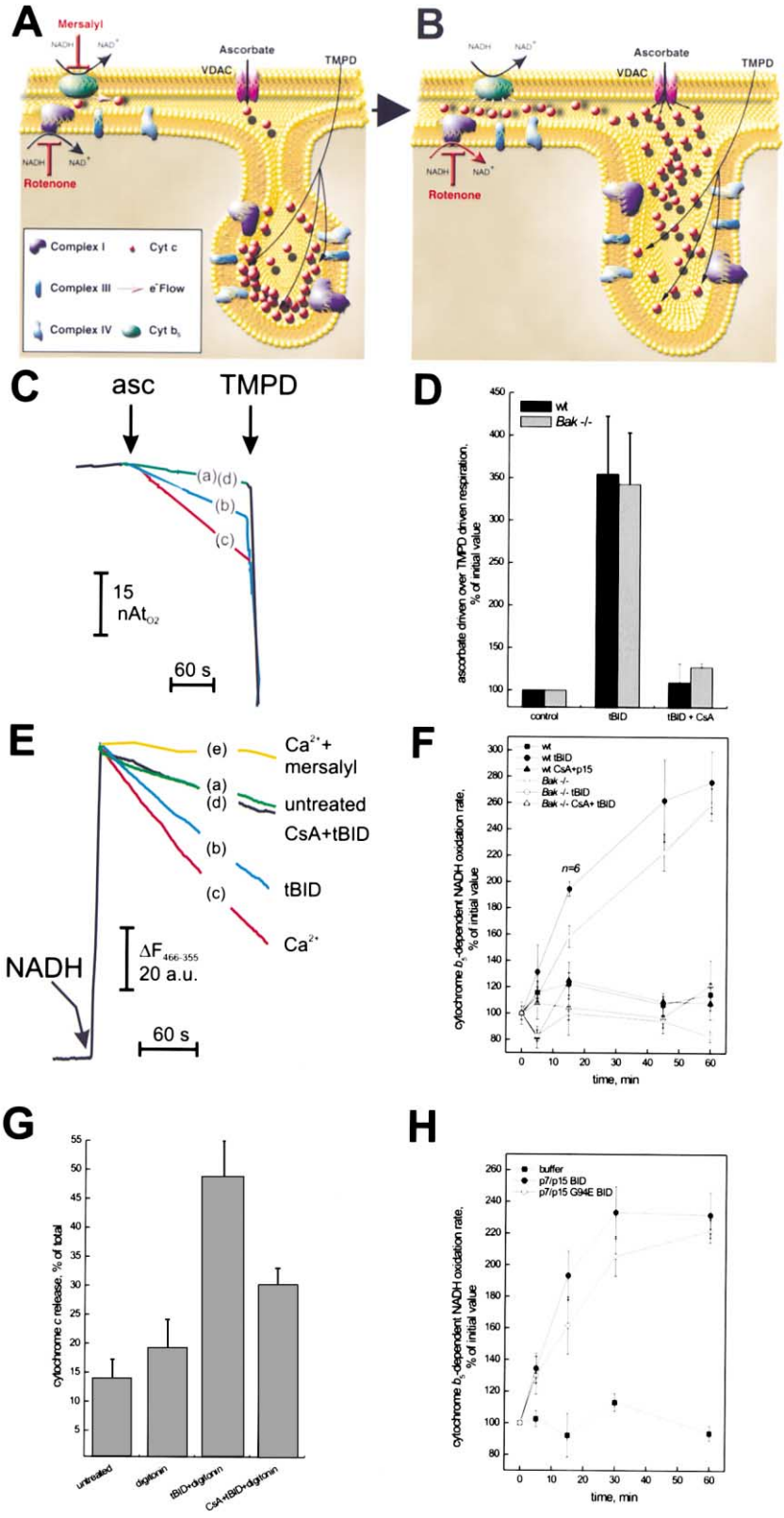

Figure 3. Effects of BID on Cytochrome *c* Mobilization in *Wt* and *Bak*$^{-/-}$ Mitochondria

(A and B) Schematic of different intramitochondrial cytochrome *c* pools and their accessibility by cytochrome b_5 or ascorbate. Symbols used are detailed in the cartoon legend.

(C) Representative traces of ascorbate-driven respiration. 1 mg mitochondria was incubated with 200 nmol Ca^{2+} × mg protein^{-1} (c) or with tBID (b and d). (a) No additions. In (d), mitochondria were preincubated for 2 min with 800 pmol CsA × mg protein^{-1}. After 15 min, mitochondria

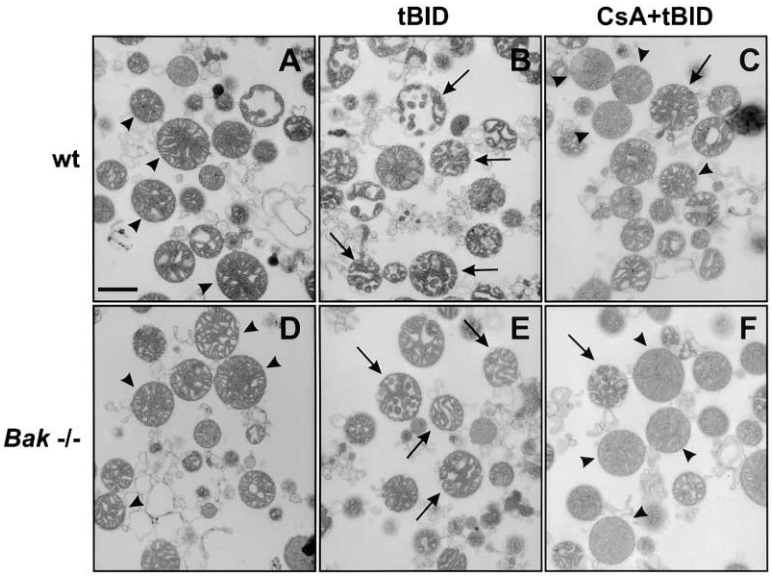

Figure 4. Transmission Electron Microscopy of tBID-Treated *Wt* and *Bak*$^{-/-}$ Mitochondria

Wt (A–C) and *Bak*$^{-/-}$ (D–F) mitochondria (0.5 mg) were incubated with tBID for 5 min (B and C; E and F). In the experiments of (C) and (F), mitochondria were pretreated for 2 min with 800 pmol × mg protein^{-1} CsA. The scale bar represents 500 nm. Representative mitochondria with class I morphology (arrowhead) and class II morphology (arrow) are noted.

6B′, and 6C′, respectively. The pleomorphic cristae are connected to the inner boundary membrane by narrow, tubular junctions in class I mitochondria (Figure 6A′). In contrast, in class II mitochondria, the cristae compartment undergoes a dramatic remodeling. The individual cristae appear fused into what is perhaps a single or a few large compartments (Figure 6B′), and the cristae junctions are widened markedly. The "crowded" appearance inside class II mitochondria is due to the extreme interconnectivity of the intracristal space, which was documented during the tracing and rendering procedure. Moreover, the curvature of the IM that outlines the cristae is frequently concave, facing the matrix in class II but convex in class I mitochondria. The relative volume occupied by the matrix space versus the intracristal space was computationally estimated (SPIDER) from the tomograms of reconstructed class I and II mitochondria. Matrix space accounted for 75%–80% of the total volume of the class I compared to 80%–85% of the class II mitochondria, providing further evidence that the remodeling of the latter is not simply a condensed, hypercontracted state.

Rotation of EM tomographic reconstructions reveals the cristae junctions at the level of the inner membrane boundary, which are presented in Figures 6A′′–C′′. Measurements indicate the average diameter of cristae junctions is 18.6 ± 2.5 nm for class I mitochondria (Figure 6A′′, yellow arrow), which has expanded to extremely elongated, ellipsoidal openings of 56.6 ± 7.7 nm ($p = 0.008$ Student's t test; range up to 71 nm) in class II mitochondria (Figure 6B′′, blue arrow). Reconstructed class III mitochondria reveal an asymmetric herniation of matrix, which distends the IM on one side with rupture of the OM at that site. Cristae structures are lost in the herniated region where the IM has unfolded (Figure 6C′). The remaining cristae junctions also provide a wider opening between the cristae and the IM (Figure 6C′′, blue open arrow).

Remodeled Class II Mitochondria Occur In Vivo Following Diverse Apoptotic Signals in *Bax, Bak*-Deficient Cells

In intact cells, two "multidomain" proapoptotic molecules, BAK and BAX, are utilized to release cytochrome *c* from mitochondria following multiple apoptotic stimuli (Wei et al., 2001). Thus, *Bax, Bak* doubly deficient (DKO)

were treated with antimycin A and CCCP, transferred into an oxygen electrode chamber, and after 2 min, oxygen recordings were started. Arrows, 6 mM ascorbate-Tris and 300 μM TMPD were added.

(D) Effects of tBID on the ratio of ascorbate over TMPD-driven respiration in *wt* (black bar) and *Bak*$^{-/-}$ (gray bar) mitochondria. The experiments were conducted exactly as in (C). Data represent mean ± SD of three different experiments.

(E) Representative traces of NADH fluorescence changes caused by cytochrome b_5-dependent NADH oxidation. 1 mg mitochondria was incubated with 200 nmol Ca^{2+} × mg protein^{-1} (c and e), or with tBID (b and d). (d) Mitochondria were preincubated for 2 min with 800 pmol CsA × mg protein^{-1}. (a) No additions. After 15 min, respiratory chain inhibitors were added, and after another 2 min, NADH fluorescence reading was started. Arrow, 20 nmol NADH × mg protein^{-1}. In (e), 200 nmol mersalyl × mg protein^{-1} was added 1 min before NADH.

(F) Time course of the effects of tBID on cytochrome b_5-dependent NADH oxidation. *Wt* (closed symbols) and *Bak*$^{-/-}$ (open symbols) mitochondria were incubated for the indicated time with tBID (circles and triangles). Triangles, mitochondria were pretreated with 800 pmol × mg protein^{-1} CsA for 2 min before the addition of tBID. Squares, no additions. Unless noted, data represent mean ± SD of three different experiments.

(G) Effects of tBID on the digitonin-releasable cytochrome *c* pool in *Bak*$^{-/-}$ mitochondria. Mitochondria were treated with 80 pmol digitonin × mg protein^{-1} for 5 min after incubation with tBID for 45 min if noted. Where indicated, mitochondria were pretreated with 800 pmol CsA × mg protein^{-1} for 3 min prior to the addition of tBID.

(H) Effects of a G94E BID mutant on cytochrome b_5-dependent NADH oxidation. The experiment was performed as in (F), except that wt (closed circle) and G94E (open circle) p7/p15 caspase-cleaved BID complex was used.

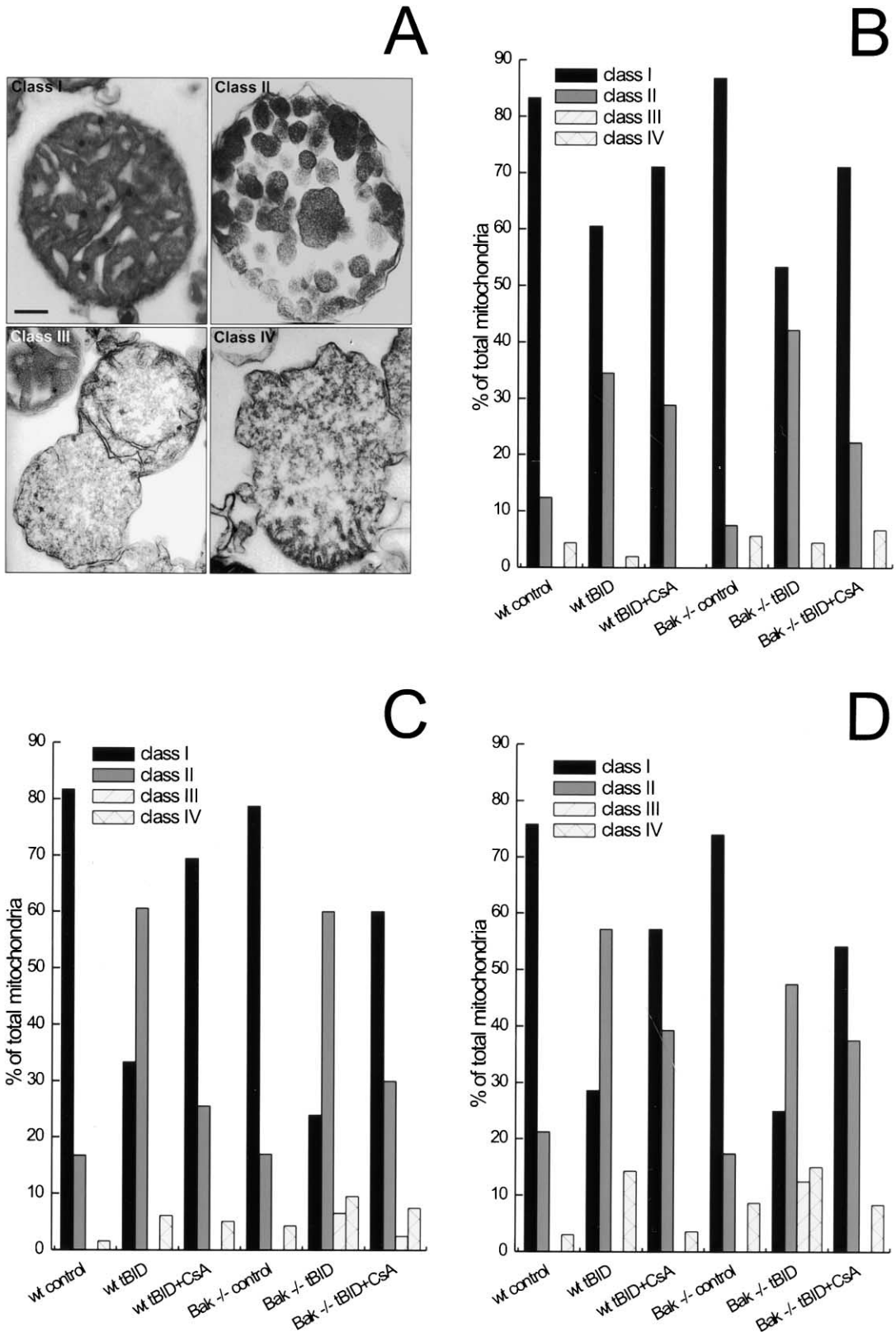

Figure 5. Morphometric Analysis of tBID Effects on *Wt* and *Bak*$^{-/-}$ Mitochondria

(A) Representative TEM of class I–IV mitochondria.

(B–D) Morphometric analysis of mitochondria. Where indicated, 0.5 mg *wt* and *Bak*$^{-/-}$ mitochondria were incubated with tBID. Where indicated, mitochondria were pretreated for 2 min with 800 pmol × mg protein^{-1} CsA. After 2 (B), 5 (C), and 10 (D) min, mitochondria were fixed, and TEM images were taken. Morphometric analysis was performed and mitochondria were assigned to morphological classes I–IV.

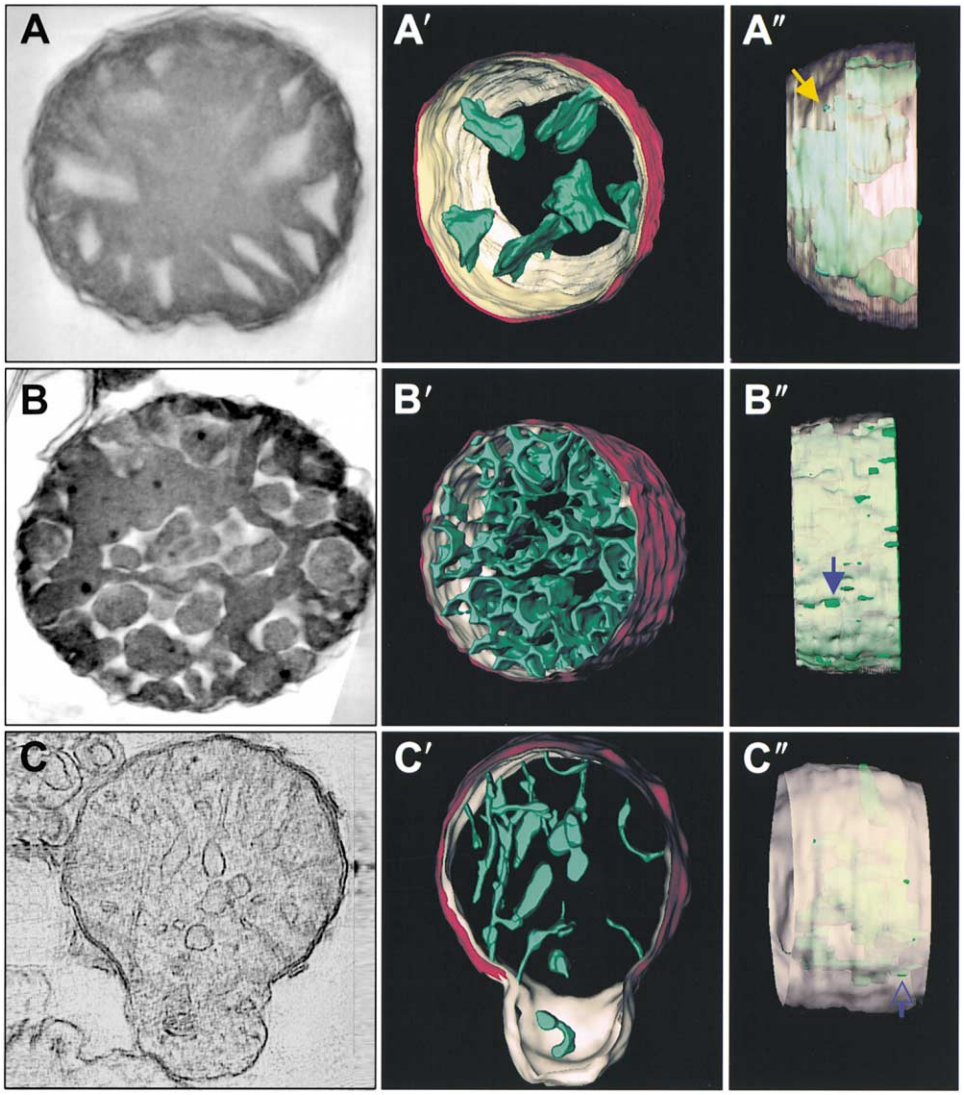

Figure 6. Electron Microscopy Tomography of Representative Class I, II, and III Mitochondria

Representative cross-sectional slice of electron microscopic tomogram of selected class I (A), class II (B), and class III (C) mitochondria. Surface-rendered views of tomographic reconstructions of each class are shown in A′, B′, and C′, respectively. The OM is depicted in red, the inner boundary membrane in yellow, and the cristae in green. Note that representative, selected cristae were traced in the class I and III mitochondria, as they were distinct. However, in the class II mitochondria, the highly interconnected cristae network had to be entirely traced. In (A′′), (B′′), and (C′′), the representative tomographic reconstructions are rotated 90° to depict the level of cristae junctions with the inner membrane boundary. Arrows indicate select cristae junctions. The dimensions of the mitochondrial reconstructions (diameter × thickness) are 930 nm × 360 nm (A), 860 nm × 450 nm (B), and 1600 nm × 310 nm (C).

cells provide an opportunity to investigate the occurrence of class II mitochondria in vivo following diverse death stimuli and assess their dependence on BAK, BAX. TEM performed 12 hr following treatment with thapsigargin, tunicamycin, brefeldin A, or heat shock revealed frequent mitochondria with class II morphology in DKO as well as wt cells (Figure 7A). The class II mitochondria are nearly identical to those noted in purified mitochondria with remodeled cristae compartments interrupted by circularized electron-dense matrix. Morphometric analysis revealed that BAX, BAK DKO cells, which are resistant to these signals, demonstrated a predominance of class II mitochondria similar to wt cells (Figure 7B).

Discussion

The mitochondrion is a highly complex and compartmentalized organelle. Cristae junctions of ~18 nm diameter physically separate the tubular cristae compartments from the narrow IMS in normal liver mitochondria. The major stores of cytochrome *c* (~85%) are sequestered within the cristae, and computer modeling of this subcompartmentalization indicates ion and ADP diffusion gradients across the cristae junctions (Mannella et al., 2001). Consequently, a major dilemma has been to explain how cytochrome *c* can be released so completely during apoptosis in the absence of gross mitochondrial swelling. Here, we identify a distinct pathway

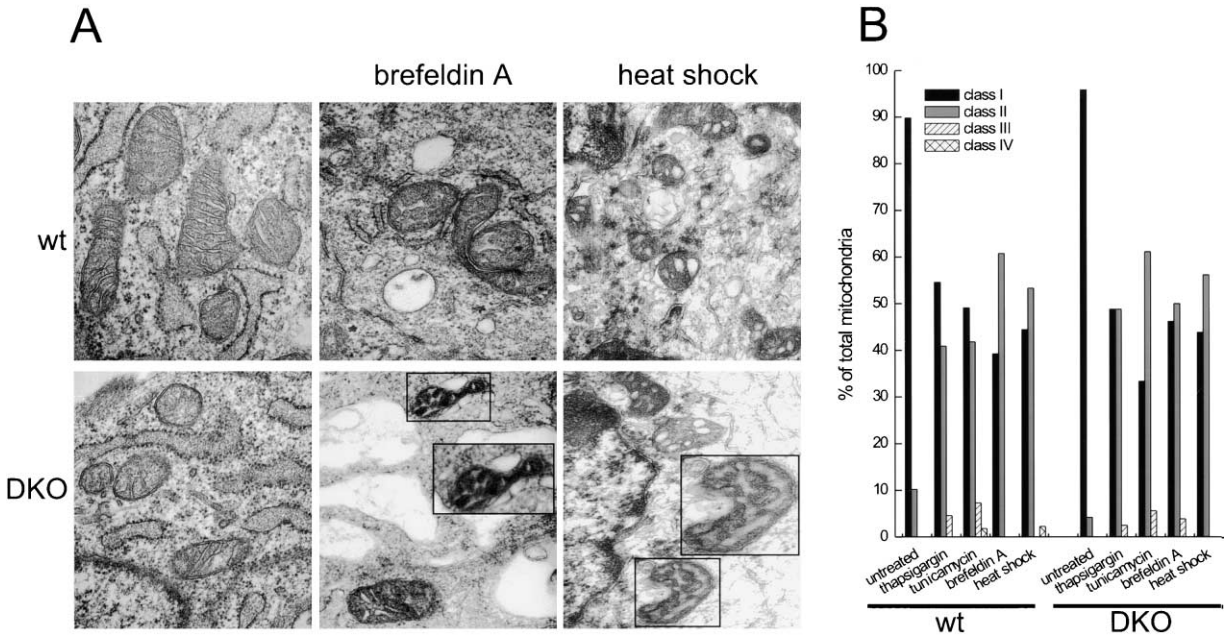

Figure 7. Mitochondrial Morphology and Morphometry in *Wt* and *Bax, Bak*-Deficient Cells Primed for Apoptosis

(A) TEM images of mitochondria in wt and *Bax, Bak*-deficient cells (DKO). Wt and DKO MEFs were treated where indicated with brefeldin A or heat shock. After 12 hr, cells were fixed and imaged. The scale bar represents 200 nm. The insets show 2× magnification of the boxed mitochondria.

(B) Morphometric analysis of mitochondria in vivo cells following death stimuli. Wt and DKO MEFs were treated with the indicated death stimulus and after 12 hr, cells were fixed, stained, and TEMs were collected. Morphometric analysis was conducted.

of mitochondrial remodeling and cytochrome *c* mobilization that could account for this rapid redistribution. Purified mitochondria, cell death genes, and pharmacologic inhibitors were used to define a program of mitochondrial remodeling that also occurs in intact cells following multiple apoptotic stimuli. A serial time course revealed a progression of inner membrane morphology that we characterized by TEM and tomographic reconstruction as recognizable stages, entitled class I–IV. A rapid transition from normal class I to the strikingly altered class II mitochondrial morphology occurs quickly, within 2–5 min after induction by an upstream "BH3-only" molecule, tBID. This mitochondrial remodeling proved independent of the BH3 domain of tBID, did not require BAK, but was inhibited by CsA. Class II mitochondria are not swollen, have an intact OM, and display a marked reorganization of cristae. Tomography reveals that individual cristae are interconnected, such that upon tracing of serial microscopic sections, cristae could no longer be individually separated, indicating they now comprise a common compartment or handful of compartments. Moreover, the cristae junctions are widened to a mean diameter of ~57 nm and range up to 71 nm, which opens the cristae space into the IMS. Consistent with this morphologic change, functional studies revealed that the entire population of cytochrome *c* was now accessible at the OM for cytochrome b_5-driven redox reactions. We propose that class II mitochondria represent a decisive step that enables the complete release of cytochrome *c* and the onset of mitochondrial dysfunction, essential for many death stimuli.

The observed remodeling of the inner membrane associated with mobilization of cytochrome *c* is generally consistent with previous reports of mitochondrial ultrastructural changes in early stages of apoptosis (Sheridan et al., 1981; Mancini et al., 1997). However, the remodeling of the inner membrane noted here (such as changes in the shape of cristae junctions) could easily be missed in the absence of 3D tomographic analysis. In another report of tomographic analysis of mitochondria during apoptosis (von Ahsen et al., 2000), no change was noted in the shape or integrity of inner or outer membranes accompanying cytochrome *c* release in extracts from *Xenopus* oocytes. However, in this experiment, mitochondria were incubated in hyperosmolar buffer, which causes mitochondria to contract to a highly condensed state (von Ahsen et al., 2000). When we incubated purified mouse liver mitochondria in hyperosmolar buffer they displayed a similar contracted morphology, but not the dramatic cristae remodeling observed here in isotonic respiratory buffer.

In retrospect, class II mitochondrial morphology was likely present in previously observed apoptotic cells. While class III morphology was particularly prominent in situ following Fas activation of hepatocytes in vivo, when we reexamined these TEMs, class II–IV mitochondria were present (Mootha et al., 2001). Early after TNF receptor engagement, most of the mitochondria display an aberrant morphology consistent with class II (Sanchez-Alcazar et al., 2001). As cytochrome *c* release following death receptor signaling can be attributed to tBID (Yin et al., 1999), these observations provide a whole-cell

setting complementary to our in vitro system. Class II mitochondria were prominent in cells following several intrinsic death stimuli (Figure 7), and just as we observed in vitro, the mitochondrial remodeling occurred independently of BAX, BAK. It is conceivable that during apoptosis, two parallel mitochondrial pathways operate, one to guarantee the release of cytochrome *c* across the OM, the other to remodel mitochondria to ensure the completeness of this release.

Increased accessibility of cytochrome *c* to the OM was previously noted following Ca^{2+}-induced mitochondrial swelling (Bernardi and Azzone, 1981). tBID, in contrast, induced redistribution in the absence of swelling and independently of BAK, indicating that actual release of cytochrome *c* across the OM was not required for remodeling. Attardi and coworkers noted that only cells primed for apoptosis by Fas activation released all stores of cytochrome *c* upon selective permeabilization of the OM by digitonin (Hajek et al., 2001). While tBID did not induce large amplitude mitochondrial swelling, it did induce transient openings of the PTP. Transient openings have been noted in isolated mitochondria and intact cells, and are not associated with swelling or $\Delta\psi_m$ collapse (Huser et al., 1998; Petronilli et al., 1999). This transient PT was coordinate with cristae remodeling and cytochrome *c* mobilization as both proved BH3 independent, BAK independent, yet CsA inhibitable. This parallel regulation suggests a common mechanism or a shared component. It has been suggested that components of the PTP reside at contact points between the IM and OM (Zoratti and Szabo, 1995). While the mobilization of cytochrome *c* would have no obvious need to involve such contact points, the striking remodeling of cristae strongly suggests that tBID has an effect on the IM. One possibility for further testing is to find whether alterations at OM/IM contacts could affect the opening of cristae junctions and the changes to IM curvature noted in class II mitochondria. The capacity of CsA to block this process suggests that its mitochondrial target, cyclophilin D (Nicolli et al., 1996), could be a functional component of this remodeling process. Alternatively, a CsA/cyclophilin D complex might affect another mitochondrial protein by analogy with the mechanism by which CsA inhibits cytosolic calcineurin (Clipstone and Crabtree, 1992). Recently, dynamin family proteins, large GTPases that generate mechanoenzymatic force on membranes, have been localized to mitochondria and shown to participate in the maintenance of mitochondrial shape including the dynamic process of fission and fusion (Margolin, 2000). Proteins that control mitochondrial shape are candidates for the apoptotic pathway (Frank et al., 2001), given the dramatic reorganization of the IM in class II mitochondria. Overall, while tBID's initial target BAK mediates release of cytochrome *c* across the OM, we propose that tBID has a second role or alternative target that mediates cristae remodeling.

Occasional class III mitochondria appear at later time points of 5 min and beyond in vitro. These mitochondria have lost volume control, displaying a herniated matrix resulting in an asymmetric bleb of expanded IM and localized rupture of the OM. The cristae appear to have unfolded into the distended IM of the bleb. The remaining cristae appear interconnected with widened cristae junctions. While class III mitochondria may reflect a progression from class II morphology, they could also be an independent stage of tBID response. Class IV mitochondria are likely an end-stage progression from class III mitochondria. The small proportion of ruptured mitochondria (class III and IV) noted in *Bak*$^{-/-}$ mitochondria in vitro appears to explain the small release of cytochrome *c* we observe at later time points (12 $\pm$ 2.2% cytochrome *c* above untreated mitochondria at 30–60 min).

The pathway of mitochondrial remodeling and transient PT initiated by tBID is genetically distinct from the actual release of cytochrome *c* across the OM, which requires BH3 of BID and the presence of BAK, but is resistant to CsA. Whether all "BH3-only" proteins will also trigger cristae remodeling deserves to be tested, as the data in Figure 7 suggests they may. The apoptotic pathway bifurcates following activation of a "BH3-only" molecule with activation of BAX, BAK resulting in the cytosolic release of cytochrome *c* and consequent caspase activity, whereas a separate path of mitochondrial remodeling insures complete release of cytochrome *c* and mitochondrial dysfunction.

Experimental Procedures

Isolation of Mitochondria, Cytochrome *c*, and Adenylate Kinase Release

Mitochondria were isolated from liver of Balb/c7 mice by standard differential centrifugation, and resuspended in isolation buffer (IB; 0.2 M sucrose, 10 mM Tris-MOPS [pH 7.4], 0.1 mM EGTA-Tris, 0.1% delipidated BSA).

For cytochrome *c* and adenylate kinase (AK) release, mitochondria (0.5 mg/ml) were incubated in experimental buffer (EB; 125 mM KCl, 10 mM Tris-MOPS [pH 7.4], 1 mM Pi, 5 mM glutamate, 2.5 mM malate, 10 μM EGTA-Tris [pH 7.4]), and treated as described at 25°C. At the indicated time, mitochondria were pelleted by centrifugation at 12000 $\times$ g at 4°C for 3 min and resuspended in the same volume of EB. Cytochrome *c* release was determined either by densitometry (Stratagene Eagle Eye II; Bio-Rad) of immunoblots, or by rat/mouse-specific ELISA performed on mitochondrial pellet and supernatant diluted 1:20 in PBS containing 0.5% Triton X-100 (R&D Systems). AK was quantified, measuring its enzymatic activity by assessing the rate of NADH oxidation at 366 nm using a Beckman DU-10 spectrophotometer. 10 μl of the supernatant or pellet was added to a reaction mixture containing 0.5 mM phosphoenolpyruvate, ATP, AMP, 1 mM NADH, and 60 units of pyruvate kinase and lactate dehydrogenase in 130 mM KCl, 6 mM $MgSO_4$, 100 mM Tris-Cl (pH 7.4). Final volume was 0.1 ml, at 25°C. Cytochrome *c* and AK release are reported as the percentage of the supernatant over the total (pellet plus supernatant).

Immunoblots

For SDS-PAGE, 20 μg of mitochondrial protein was loaded in each lane of a 12% NuPAGE (NoVex) gel. After separation, proteins were transferred onto PVDF membranes (Immobilon-P; Millipore) and membranes were probed as indicated with the following primary antibodies: anti-cytochrome *c* (Pharmingen; 1:1000); anti-BID (1:1500); and anti-BAK (Calbiochem; 1:1000). HRPO-conjugated secondary antibodies (CalTag; 1:2000) were visualized by chemiluminescence (Amersham).

Calcein Release

Mitochondria suspended in IB without BSA were loaded with 10 nmol $\times$ mg protein^{-1} calcein-AM (Molecular Probes) for 20 min at room temperature in the dark. Following two washes in IB, the calcein-loaded mitochondria were resuspended in IB at a final concentration of 10 mg/ml. 0.5 mg/ml calcein-loaded mitochondria were incubated in EB and treated as described. After the indicated time, mitochondria were pelleted. Calcein was measured in an LS-50B spectrofluorimeter (Perkin Elmer) with excitation and emission

wavelengths set at 488 ± 2.5 nm and 542 ± 2.5 nm, respectively. Calcein release is reported as the percentage of the calcein measured in the supernatant over the total (pellet plus supernatant).

Cytochrome b_5-Dependent NADH Oxidation Assay

1 mg/ml mitochondria was incubated in EB and treated as indicated. 400 pmol CCCP, 2 nmol rotenone, and 1 nmol antimycin A × mg protein^{-1} were added after the time indicated and the reaction was transferred to a cuvette. After 2 min, 10 μM NADH was added and its oxidation was monitored as the decrease in NADH fluorescence in an LS-50B spectrofluorimeter (Perkin Elmer) set with λ_{ex} = 366 nm and λ_{em} = 455 nm, with 5 nm slits.

Ascorbate/TMPD-Driven Respiration Assay

1 mg/ml mitochondria was incubated in sucrose buffer (0.2 M sucrose, 10 mM Tris-MOPS [pH 7.4], 1 mM Pi, 5 mM glutamate, 2.5 mM malate, 10 μM EGTA-Tris [pH 7.4]) and treated as indicated in the figure legends. After the indicated time, 400 pmol CCCP and 1 nmol antimycin A × mg protein^{-1} were added, and the reaction was transferred to a Clark-type oxygen electrode chamber. Final volume was 1 ml, at 25°C. After 2 min, 6 mM ascorbate was added, followed after a further 3 min by 300 μM TMPD. The ascorbate-driven O_2 consumption rate over the total TMPD-driven rate is plotted as a percentage of the ratio in the untreated mitochondria.

Mitochondrial Swelling and Membrane Potential Determination

Swelling of 0.5 mg/ml mitochondria incubated in EB was monitored by changes in side scatter at 545 ± 2.5 nm using an LS-50B spectrofluorimeter equipped with magnetic stirring at 25°C. Membrane potential changes of 0.5 mg/ml mitochondria incubated in experimental buffer were monitored from the dequenching of a 0.3 μM rhodamine 123 (Molecular Probes) solution in an LS-50B spectrofluorimeter at 25°C, using excitation and emission wavelengths set at 503 ± 2.5 nm and 525 ± 5 nm, respectively.

Purification of tBID, Wt, and G94E p7/p15 BID

tBID was generated and purified as described (Wei et al., 2000). Wt and G94E p22 BID were cleaved with recombinant caspase-8 into the active p7/p15 BID as described (Wei et al., 2000). tBID and p7/p15 BID were dialyzed against 10 mM HEPES (pH 7.6), 1 mM DTT, 125 mM KCl. Unless noted, tBID was used at a final concentration of 320 pmol × mg mitochondrial protein^{-1}, whereas p7/p15 BID was used at 3.2 pmol × mg protein^{-1}.

Transmission Electron Microscopy, Tomographic Reconstruction, and Mitochondrial Morphometry

Mitochondria were fixed for 1 hr at 25°C using glutaraldehyde dissolved in EB at a final concentration of 1.25%, embedded in plastic, sectioned, and stained with uranyl acetate and lead citrate. Thin sections were imaged on a JEOL 1200EX transmission electron microscope. For tomography, colloidal gold particles were applied to one side of 300–500 nm thick sections as alignment markers. Tilt series of 122 images were recorded on the Albany AEI EM7 MkII HVEM, operated at an acceleration voltage of 1000 kV. The images were recorded around two orthogonal tilt axes, each over an angular range of 120° with a 2° tilt interval. The double-tilt images were aligned as previously described (Penczek et al., 1995) and tomographic reconstructions were made using the weighted back projection method (Radermacher, 1992). Image processing was done using the SPIDER system. The reconstructed volumes had dimensions of 512 × 512 × 100–145 pixels depending on section thickness, with a pixel size range of 2.5–4.1 nm. Surface-rendered models were made using Sterecon (Marko and Leith, 1996) to segment the volume and Iris Explorer (NAG) for rendering. Measurements of the dimensions of cristae openings were made directly on one-pixel-thick slices from the respective tomograms.

For morphometric analysis of fields of mitochondria in thin sections, at least four different transmission EM micrographs representing different areas in the grid were selected and number-coded prints were produced at the Harvard Medical School EM Facility. Mitochondria with profile diameters <200 nm were excluded from the analysis, and in the case of mitochondria which displayed characteristics bridging morphologic classes, they were assigned to the lower class. The classification procedure was performed in a blinded fashion.

Cell Culture and Induction of Apoptosis

For apoptosis induction, MEFs were plated in 24-well plates at a density of 10^4 cells/well and grown for 24 hr (Wei et al., 2001). Apoptosis was initiated by 2 μM thapsigargin, 2 μg/ml brefeldin A, 1 μg/ml tunicamycin or by 5 hr of heat shock (43°C in a humidified atmosphere of 95% air, 5% CO_2). Apoptosis was detected by flow cytometric detection of annexin V staining (BD Pharmingen) 24 hr after the induction of cell death.

Acknowledgments

L.S. is a recipient of the Human Frontier Science Program Long-Term Fellowship. S.A.O. is supported by NIH Physician Training grant #T32-HL07627-16. Electron tomography work at the Resource for the Visualization of Biological Complexity is supported by the National Center for Research Resources, NIH grant #RR01219. This work was supported in part by NIH grant #CA50239-14.

Received July 11, 2001; revised December 3, 2001.

References

Bernardi, P. (1999). Mitochondrial transport of cations: channels, exchangers and permeability transition. Physiol. Rev. *79*, 1127–1155.

Bernardi, P., and Azzone, G.F. (1981). Cytochrome c as an electron shuttle between the outer and inner mitochondrial membranes. J. Biol. Chem. *256*, 7187–7192.

Bernardi, P., Scorrano, L., Colonna, R., Petronilli, V., and Di Lisa, F. (1999). Mitochondria and cell death. Mechanistic aspects and methodological issues. Eur. J. Biochem. *264*, 687–701.

Cheng, E.H., Wei, M.C., Weiler, S., Flavell, R.A., Mak, T.W., Lindsten, T., and Korsmeyer, S.J. (2001). BCL-2, BCL-X_L sequester BH3 domain-only molecules preventing BAX- and BAK-mediated mitochondrial apoptosis Mol. Cell *8*, 705–711.

Clipstone, N.A., and Crabtree, G.R. (1992). Identification of calcineurin as a key signalling enzyme in T-lymphocyte activation. Nature *357*, 695–697.

Eskes, R., Antonsson, B., Osen-Sand, A., Montessuit, S., Richter, C., Sadoul, R., Mazzei, G., Nichols, A., and Martinou, J.-C. (1998). Bax-induced cytochrome c release from mitochondria is independent of the permeability transition pore but highly dependent on Mg^{2+} ions. J. Cell Biol. *143*, 217–224.

Frank, S., Gaume, B., Bergmann-Leitner, E.S., Leitner, W.W., Robert, E.G., Catez, F., Smith, C.L., and Youle, R.J. (2001). The role of dynamin-related protein *1*, a mediator of mitochondrial fission, in apoptosis. Dev. Cell *1*, 515–525.

Frey, T.G., and Mannella, C.A. (2000). The internal structure of mitochondria. Trends Biochem. Sci. *25*, 319–324.

Goldstein, J.C., Waterhouse, N.J., Juin, P., Evan, G.I., and Green, D.R. (2000). The coordinate release of cytochrome c during apoptosis is rapid, complete and kinetically invariant. Nat. Cell Biol. *2*, 156–162.

Green, D.R., and Reed, J.C. (1998). Mitochondria and apoptosis. Science *281*, 1309–1312.

Hackenbrock, C.R. (1966). Ultrastructural bases for metabolically linked mechanical activity in mitochondria. I. Reversible ultrastructural changes with change in metabolic steady state in isolated liver mitochondria. J. Cell Biol. *30*, 269–297.

Hajek, P., Villani, G., and Attardi, G. (2001). Rate-limiting step preceding cytochrome c release in cells primed for Fas-mediated apoptosis revealed by analysis of cellular mosaicism of respiratory changes. J. Biol. Chem. *276*, 606–615.

Hoppel, C., and Cooper, C. (1968). The action of digitonin on rat liver mitochondria. The effects on enzyme content. Biochem. J. *107*, 367–375.

Huser, J., Rechenmacher, C.E., and Blatter, L.A. (1998). Imaging the permeability pore transition in single mitochondria. Biophys. J. *74*, 2129–2137.

Kluck, R.M., Esposti, M.D., Perkins, G., Renken, C., Kuwana, T., Bossy-Wetzel, E., Goldberg, M., Allen, T., Barber, M.J., Green, D.R., and Newmeyer, D.D. (1999). The pro-apoptotic proteins, Bid and Bax, cause a limited permeabilization of the mitochondrial outer membrane that is enhanced by cytosol. J. Cell Biol. *147*, 809–822.

Kroemer, G., Dallaporta, B., and Resche-Rigon, M. (1998). The mitochondrial death/life regulator in apoptosis and necrosis. Annu. Rev. Physiol. *60*, 619–642.

Lehninger, A.L. (1951). Phosphorylation coupled to oxidation of dihydrodiphosphopyridine nucleotide. J. Biol. Chem. *190*, 345–359.

Lemasters, J.J., Nieminen, A.L., Qian, T., Trost, L., Elmore, S.P., Nishimura, Y., Crowe, R.A., Cascio, W.E., Bradham, C.A., Brenner, D.A., and Herman, B. (1998). The mitochondrial permeability transition in cell death: a common mechanism in necrosis, apoptosis and autophagy. Biochim. Biophys. Acta *1366*, 177–196.

Li, P., Nijhawan, D., Budihardjo, I., Srinivasula, S.M., Ahmad, M., Alnemri, E.S., and Wang, X. (1997). Cytochrome c and dATP-dependent formation of Apaf-1/caspase-9 complex initiates an apoptotic protease cascade. Cell *91*, 479–489.

Luo, X., Budihardjo, I., Zou, H., Slaughter, C., and Wang, X. (1998). Bid, a Bcl2 interacting protein, mediates cytochrome c release from mitochondria in response to activation of cell surface death receptors. Cell *94*, 481–490.

Mancini, M., Anderson, B.O., Caldwell, E., Sedghinasab, M., Paty, P.B., and Hockenbery, D.M. (1997). Mitochondrial proliferation and paradoxical membrane depolarization during terminal differentiation and apoptosis in a human colon carcinoma cell line. J. Cell Biol. *138*, 449–469.

Mannella, C.A., Pfeiffer, D.R., Bradshaw, P.C., Moraru, I.I., Slepchenko, B., Loew, L.M., Hsieh, C., Buttle, K., and Marko, M. (2002). Topology of the mitochondrial inner membrane: dynamics and bioenergetic implications. IUBMB Life, *52*, 1–7.

Margolin, W. (2000). Organelle division: self-assembling GTPase caught in the middle. Curr. Biol. *10*, R328–R330.

Marko, M., and Leith, A. (1996). Sterecon—three-dimensional reconstructions from stereoscopic contouring. J. Struct. Biol. *116*, 93–98.

Mootha, V.K., Wei, M.C., Buttle, K.F., Scorrano, L., Panoutsakopoulou, V., Mannella, C.A., and Korsmeyer, S.J. (2001). A reversible component of mitochondrial respiratory dysfunction in apoptosis can be rescued by exogenous cytochrome c. EMBO J. *20*, 661–671.

Nicholls, P., Hildebrandt, V., Hill, B.C., Nicholls, F., and Wrigglesworth, J.M. (1980). Pathways of cytochrome *c* oxidation by soluble and membrane-bound cytochrome *aa*3. Can. J. Biochem. *58*, 969–977.

Nicolli, A., Basso, E., Petronilli, V., Wenger, R.M., and Bernardi, P. (1996). Interactions of cyclophilin with the mitochondrial inner membrane and regulation of the permeability transition pore, a cyclosporin A-sensitive channel. J. Biol. Chem. *271*, 2185–2192.

Penczek, P., Marko, M., Buttle, K., and Frank, J. (1995). Double-tilt electron tomography. Ultramicroscopy *60*, 393–410.

Perotti, M.E., Anderson, W.A., and Swift, H. (1983). Quantitative cytochemistry of the diaminobenzidine cytochrome oxidase reaction product in mitochondria of cardiac muscle and pancreas. J. Histochem. Cytochem. *31*, 351–365.

Petronilli, V., Szabo, I., and Zoratti, M. (1989). The inner mitochondrial membrane contains ion-conducting channels similar to those found in bacteria. FEBS Lett. *259*, 137–143.

Petronilli, V., Miotto, G., Canton, M., Colonna, R., Bernardi, P., and Di Lisa, F. (1999). Transient and long-lasting openings of the mitochondrial permeability transition pore can be monitored directly in intact cells by changes of mitochondrial calcein fluorescence. Biophys. J. *76*, 725–734.

Radermacher, M. (1992). Weighted back-projection methods. In Electron Tomography, J. Frank, ed. (New York: Plenum), pp. 91–115.

Sanchez-Alcazar, J.A., Schneider, E., Martinez, M.A., Carmona, P., Hernandez-Munoz, I., Siles, E., De La Torre, P., Ruiz-Cabello, J., Garcia, I., and Solis-Herruzo, J.A. (2001). Tumor necrosis factor-alpha increases the steady-state reduction of cytochrome b of the mitochondrial respiratory chain in metabolically inhibited L929 cells. J. Biol. Chem. *275*, 13353–13361.

Sheridan, J.W., Bishop, C.J., and Simmons, R.J. (1981). Biophysical and morphological correlates of kinetic change and death in a starved human melanoma cell line. J. Cell Sci. *49*, 119–137.

Shimizu, S., and Tsujimoto, Y. (2000). Proapoptotic BH3-only Bcl-2 family members induce cytochrome c release, but not mitochondrial membrane potential loss, and do not directly modulate voltage-dependent anion channel activity. Proc. Natl. Acad. Sci. USA *97*, 577–582.

Single, B., Leist, M., and Nicotera, P. (1998). Simultaneous release of adenylate kinase and cytochrome c in cell death. Cell Death Differ. *5*, 1001–1003.

von Ahsen, O., Renken, C., Perkins, G., Kluck, R.M., Bossy-Wetzel, E., and Newmeyer, D.D. (2000). Preservation of mitochondrial structure and function after Bid- or Bax-mediated cytochrome c release. J. Cell Biol. *150*, 1027–1036.

Wei, M.C., Lindsten, T., Mootha, V.K., Weiler, S., Gross, A., Ashiya, M., Thompson, C.B., and Korsmeyer, S.J. (2000). tBID, a membrane-targeted death ligand, oligomerizes BAK to release cytochrome c. Genes Dev. *14*, 2060–2071.

Wei, M.C., Zong, W.X., Cheng, E.H., Lindsten, T., Panoutsakopoulou, V., Ross, A.J., Roth, K.A., MacGregor, G.R., Thompson, C.B., and Korsmeyer, S.J. (2001). Proapoptotic BAX and BAK: a requisite gateway to mitochondrial dysfunction and death. Science *292*, 727–730.

Yin, X.M., Wang, K., Gross, A., Zhao, Y., Zinkel, S., Klocke, B., Roth, K.A., and Korsmeyer, S.J. (1999). Bid-deficient mice are resistant to Fas-induced hepatocellular apoptosis. Nature *400*, 886–891.

Zha, J., Weiler, S., Oh, K.J., Wei, M.C., and Korsmeyer, S.J. (2000). Posttranslational N-myristoylation of BID as a molecular switch for targeting mitochondria and apoptosis. Science *290*, 1761–1765.

Zong, W.X., Lindsten, T., Ross, A.J., MacGregor, G.R., and Thompson, C.B. (2001). BH3-only proteins that bind pro-survival Bcl-2 family members fail to induce apoptosis in the absence of Bax and Bak. Genes Dev. *15*, 1481–1486.

Zoratti, M., and Szabo, I. (1995). The mitochondrial permeability transition. Biochim. Biophys. Acta *1241*, 139–176.